Contents lists available at ScienceDirect

Biochemistry and Biophysics Reports

A novel immune-related prognostic model with surgical status to predict tumor immune cell infiltration and drug sensitivity in head and neck squamous cell carcinoma

Lang Wang [a,1], Xianchao Yu [b,1], Hongwei Li [c,1], Chenglong Wang [a,*]

[a] Department of Radiology, West China School of Public Health and West China Fourth Hospital, Sichuan University, Chengdu, Sichuan Province, 610041, PR China
[b] School of Life Science and Technology, University of Electronic Science and Technology of China, Chengdu, Sichuan Province, 611731, PR China
[c] Department of Radiology, The Third Hospital of Mianyang, Sichuan Mental Health Center, Mianyang, Sichuan Province, 621000, PR China

ABSTRACT

Tumor-infiltrating immune cells (TICs) affect tumorigenesis and tumor development in head and neck squamous cell carcinoma (HNSCC). We constructed a novel predictive model for HNSCC based on immune-related genes (IRGs) from The Cancer Genome Atlas and the Immunology Database and Analysis Portal. After identifying the IRGs, a predictive model involving 13 IRGs with high stratification value of overall survival (OS) was constructed by multiple support vector machine recursive feature elimination and least absolute shrinkage and selection operator regression. We explored the relationship between the risk score (RS) and clinical characteristics. The nomogram showed high concordance and good agreement in OS. Four TICs affected the OS and were in agreement with the abundance analysis of the RS levels. Furthermore, the low-risk HNSCC group showed higher expression of PD-1, CTLA4, and TIGIT, while the high-risk group showed higher expression of EGFR. The high-risk HNSCC showed high sensitivity to eight drugs.

1. Introduction

Head and neck squamous cell carcinoma (HNSCC), which mainly involves the oral cavity, sinonasal cavity, pharynx, and larynx, is among the top ten original malignancies by incidence worldwide. It has been associated with human papillomavirus infection and heavy tobacco and alcohol use [1,2]. The incidence of HNSCC in 2020 was over 800,000 new cases worldwide, with over 400,000 deaths. Such high rates place clinical and economic burdens on the public health system. Males have substantially higher incidence and mortality rates than females [3,4]. Although multi-modal treatments such as surgery, chemotherapy, radiotherapy, and immune checkpoint inhibitors (ICI) were used in patients with HNSCC, the overall survival (OS) remains disappointing, especially in those with locally-advanced lesions [5]. Hence, investigating the molecular mechanisms and potential biological markers associated with HNSCC tumorigenesis, disease progression, and treatment response remains challenging but presents opportunities for a better understanding of the disease [6].

The tumor microenvironment (TME) is a complex entity that plays an important role in HNSCC tumorigenesis and tumor growth, progression, and treatment response. It includes the extracellular matrix, cancer-associated fibroblasts, and various tumor-infiltrating immune cell (TIC) subtypes [7,8]. TICs interact with tumor cells to form a supporting environment and produce hormone-like bioregulators to affect homeostasis locally and systematically, preventing the body's anticancer activity and enhancing tumor growth [9]. TICs are also strongly associated with the expression of most immune checkpoints in HNSCC [10] and could potentially impact the response to immunotherapy. As a well-known tumor type with a strong immune infiltration response [11], immune-related signatures were used to predict the prognosis, immune checkpoint expression, TIC levels, and various response states after ICI treatment in HNSCC [12,13]. Immune-related signatures were more accurate in predicting OS than prediction models based on glycosyltransferase and fatty acid metabolism-related signatures [10,14]. Screening for further immune-related signatures and developing TIC prediction tools could improve outcome evaluation in HNSCC and lead
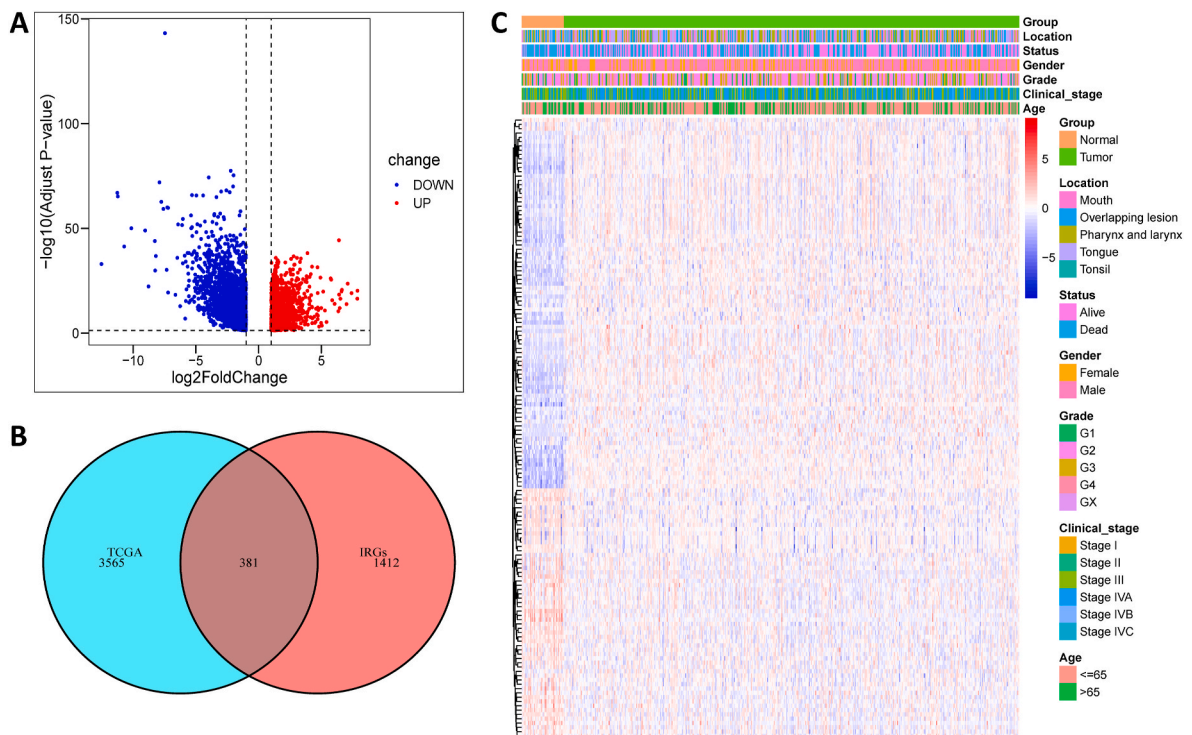
Fig. 1. Screening for immune-related DEGs in HNSCC. (A) Volcano plot showing DEGs between tumor and normal samples according to TCGA-HNSCC cohort. (B) Venn plot showing the intersection analysis of DEGs with IRGs from the ImmPort database. (C) Heat map of immune-related DEGs with clinical characteristics.
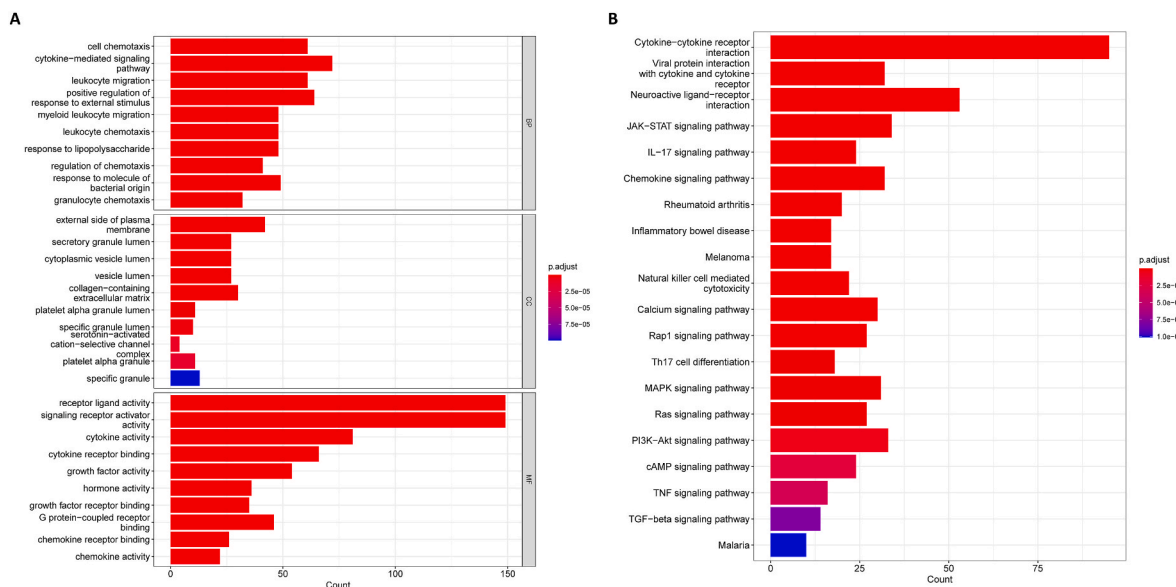

Fig. 2. Functional enrichment analyses for immune-related DEGs. (A) GO enrichment analysis. (B) KEGG pathway analysis.

to better clinical and therapeutic strategies.

However, surgery and radiochemotherapy could substantially disrupt tissues and vessels and change the TIC component in HNSCC, exacerbating preexisting immunosuppressive effects [5,7]. The OS prediction accuracy of previously published models was established based on immune-related signatures, and the usefulness of tumor stage and grade was limited in patients with HNSCC. Moreover, the surgical status, including perineural invasion and positive margin, could also affect the HNSCC outcome [15]. The prediction efficacy of combining immune-related markers with surgical status remains unclear. This study's aims were: (1) screening and identifying novel immune-related

signatures based on differentially-expressed genes (DEGs) and the construction of a predictive model with high concordance and good fitting; (2) validation and evaluation of the predictive model for survival outcomes, risk stratification, surgical status, and treatment response, and the construction of a novel nomogram model; (3) prediction of TIC abundance, immunotherapy targets, and drug sensitivity using risk scores (RSs) based on immune-related genes (IRGs) to achieve a comprehensive understanding of the immune response and improve therapeutic decision-making for HNSCC.

Table 1
Cox regression analysis for screening of immune-related DEGs of prognosis for HNSCC.

Gene	Univariate-cox analysis HR(95%CI)	p-value
MPO	3.109(1.174-8.235)	0.022
HTN1	1.548(1.010-2.372)	0.045
FAM3D	0.881(0.786-0.987)	0.029
SLC11A1	1.314(1.002-1.723)	0.048
GAST	1.154(1.028-1.296)	0.015
PPARG	1.292(1.015-1.646)	0.037
STC2	1.221(1.041-1.432)	0.014
BLNK	0.818(0.680-0.982)	0.031
INHBA	1.124(1.009-1.253)	0.034
ACTA1	1.054(1.007-1.105)	0.025
CXCL13	0.898(0.809-0.997)	0.044
GDF7	0.067(0.008-0.539)	0.011
SPP1	1.072(1.001-1.149)	0.047
ULBP2	1.225(1.032-1.453)	0.020
TNFRSF19	0.797(0.653-0.974)	0.026
IL34	0.827(0.693-0.988)	0.036
AQP9	1.212(1.021-1.440)	0.028
TFRC	1.181(1.020-1.367)	0.026
TNFRSF4	0.724(0.576-0.911)	0.006
OLR1	1.271(1.115-1.448)	0.000
AVPR2	0.429(0.198-0.930)	0.032
PTX3	1.164(1.005-1.347)	0.042
SCGB3A1	0.901(0.814-0.996)	0.042
DES	1.062(1.012-1.114)	0.014
NTF3	0.630(0.399-0.994)	0.047
TNFRSF18	0.869(0.762-0.991)	0.037
CHGB	1.182(1.082-1.290)	0.000
DKK1	1.169(1.057-1.292)	0.002
FGF14	3.980(1.590-9.960)	0.003
CCL26	1.131(1.016-1.259)	0.024
CD79A	0.869(0.788-0.960)	0.005
PCSK2	1.532(1.149-2.041)	0.004
CD19	0.687(0.523-0.902)	0.007
IL21	0.083(0.009-0.797)	0.031
SFTPA2	1.358(1.060-1.741)	0.016
IL1F10	0.758(0.585-0.983)	0.037
OXT	0.372(0.156-0.888)	0.026
CGB2	2.555(1.024-6.372)	0.044
CALCA	2.790(1.642-4.739)	0.000
NR0B1	1.498(1.177-1.906)	0.001

HR = hazard ratio; CI=Confidence interval.

Table 2
The clinical characteristics of included patients of TCGA database.

Clinical characteristics		Total Number(n = 472)	Training Set (n = 323)	Test Set (n = 149)	p-value
Age	<=60yr	231	160	71	0.7782
	>60yr	241	163	78	
Sex	Female	128	82	46	0.2566
	Male	344	241	103	
Stage	Stage I	19	10	9	0.1143
	Stage II	92	67	25	
	Stage III	102	75	27	
	Stage IVA	246	165	81	
	Stage IVB/IVC	13	6	7	
Grade	G1	53	34	19	0.7068
	G2	287	194	93	
	G3/G4	116	84	32	
	Gx	16	11	5	
Location	Mouth	105	67	38	0.3403
	Overlapping lesion	68	45	23	
	Pharynx and larynx	125	87	38	
	Tongue	136	101	35	
	Tonsil	38	23	15	

2. Materials and methods

2.1. Data source and processing

The HTSeq-counts and FPKM data of patients with HNSCC in The Cancer Genome Atlas (TCGA) database and their clinical characteristics and survival data (accessed on 18 January 2023) were downloaded from the UCSC Xena website (https://xenabrowser.net/datapages/). We acquired RNA-sequencing transcriptome data for 539 cases, including 495 tumor and 44 normal samples. After removing those with incomplete or missing survival data, the survival analysis included 472 patients with HNSCC. Ethical approval and patient informed consent were unnecessary because all the data were from a publicly available database.

2.2. Identification of immune-related DEGs

We analyzed DEGs between normal and tumor tissues in patients with HNSCC using the 'DESeq2' package in R software, setting |log2FC| > 1 and a false discovery rate <0.05. A volcano plot of the DEGs was generated by the 'ggpubr' package. We downloaded IRG data from the Immunology Database and Analysis Portal (ImmPort) database (https://www.immport.org/home; accessed on 18 January 2023). Immune-related DEGs were detected by intersecting the DEGs and IRGs. The 'VennDiagram' and 'heatmap' packages were used to visualize this intersection.

2.3. Functional enrichment analysis

We used the 'clusterProfiler' package to perform functional analysis based on Gene Ontology (GO) and the Kyoto Encyclopedia of Genes and Genomes (KEGG), setting the adjusted p-value threshold at <0.05. GO enrichment analysis included three biological categories: biological processes, cellular components, and molecular functions.

2.4. A prognostic prediction model for HNSCC

After arranging the survival data, immune-related DEG expression levels, and clinic characteristics, we randomly divided the cohort into a Training Set (2/3) and a Test Set (1/3), with sample sizes of 323 and 149, respectively.

To develop a prognostic prediction model with high concordance, we first performed univariate Cox regression analysis in the Training Set to acquire the genes related to HNSCC prognosis using the 'survival' package ($p < 0.05$). Subsequently, least absolute shrinkage and selection operator (LASSO) regression and multiple support vector machine recursive feature elimination (mSVM-RFE) were performed to screen genes using the 'glmnet' and 'e1071' packages, respectively. The mSVM-RFE algorithm is widely used for accurate predictions based on complex gene expression data [16]. The gene selection results by LASSO regression in various lambda values of the cross-validation error and the mSVM-RFE algorithm results were recorded and combined to calculate the concordance index (C-index). Finally, the gene types with the highest C-index were selected to construct the prognostic prediction model. We calculated the RS for each sample and then divided the cohort into high-risk and low-risk HNSCC using the median RS as a cutoff value. These groups were visualized using the 'ggrisk' package. We used the 'survminer' and 'timeROC' packages to perform Kaplan-Meier (K-M) and time-dependent receiver operating characteristic (ROC) curve analyses, respectively, and evaluate the prognostic efficacy of the constructed prediction model, using the Training, Test, and combined (all samples) sets. To investigate the relationship between tumor cell-intrinsic genes and identified IRGs, we performed a correlation analysis between the expression of cancer driver genes and RS. We screened the top ten cancer driver genes of HNSCC using the Integrative Onco-Genomics database (https://www.intogen.org/search). *TP53, FAT1, NOTCH1, CSMD3, PIK3CA, CDKN2A, LRP1B, KMT2D, CASP8* and
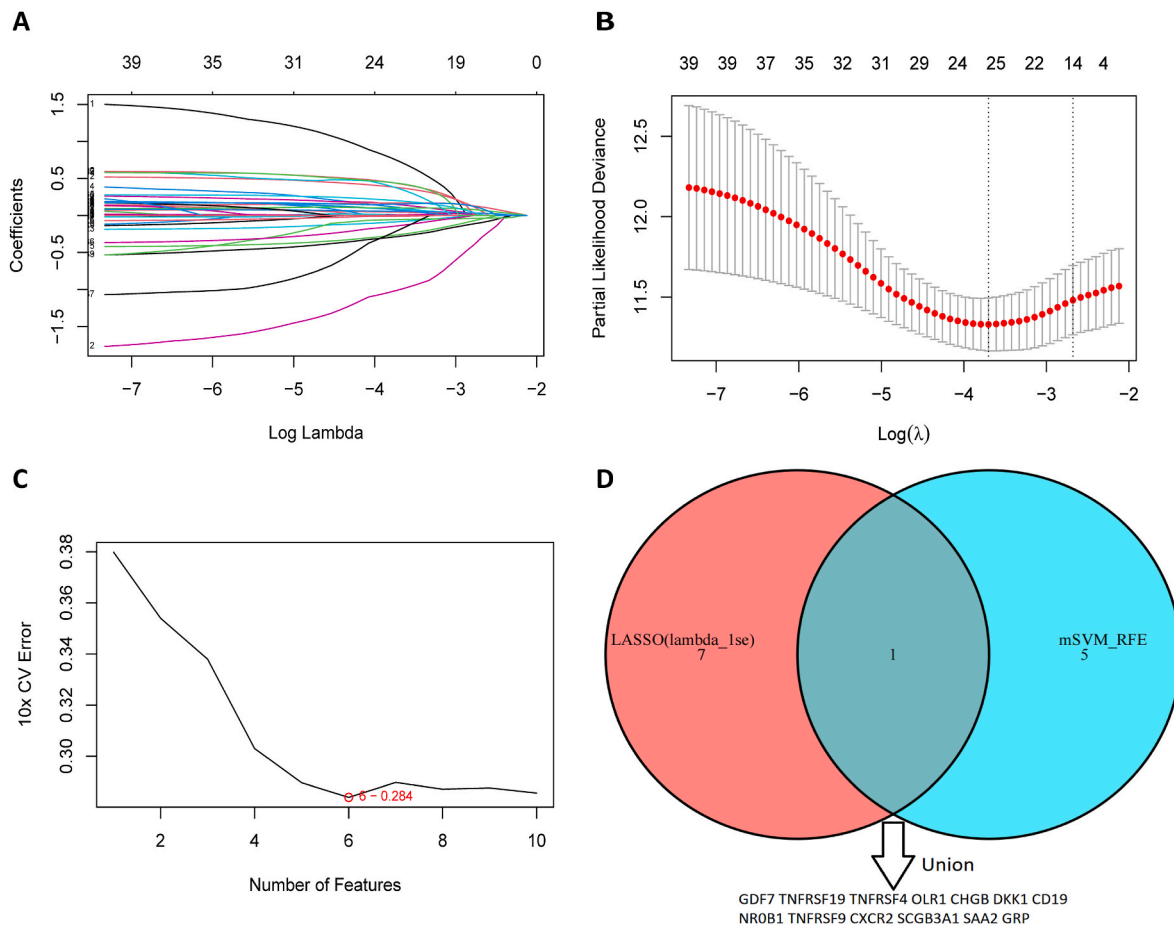
Fig. 3. LASSO regression and mSVM-RFE algorithm for genes selection. (A,B) LASSO regression complexity was controlled by lambda. (C) mSVM-RFE algorithm by 10-fold cross-validation. (D) The union analysis of LASSO regression (λ = 1se) and mSVM-FRE.

Table 3
The Coefficients of each gene of the present regression model.

Gene	Coefficient
GDF7	-0.87735
TNFRSF19	-0.33183
TNFRSF4	-0.76801
OLR1	0.25134
CHGB	0.18523
DKK1	0.08212
CD19	-0.05529
NR0B1	0.45320
TNFRSF9	0.52887
CXCR2	0.14787
SCGB3A1	-0.07502
SAA2	0.15725
GRP	0.18074

NSD1 were included.

2.5. Relationship between the RS and clinical characteristics

In this part, we compared the RS in various tumor grades, origins, stages, ages, sexes, perineural invasiveness, and treatment responses. These comparisons were visualized by the 'ggpubr' package. The K-M curves were constructed using the 'survival' package based on sex, resection margin, perineural invasion, radiation therapy, and treatment response to further analyze the survival difference between the high-risk and low-risk HNSCC groups.

2.6. Construction and validation of the nomogram

To confirm the independent risk factors of HNSCC prognosis, we performed univariate and multivariate Cox regression analyses on the RS, clinical characteristics, and surgical status using the 'survival' package. Subsequently, a nomogram model, a calibration curve, and a C-index analysis were executed using the 'rms' package.

2.7. Analysis of immune cell infiltration

The proportions of 22 TICs in the HNSCC cohort were calculated using the CIBERSORT algorithm and the 'preprocessCore' package. This algorithm can characterize complex tissue cell composition based on its gene expression profile without additional histopathological analysis [17]. The relationships between the TIC subtypes and the RS were assessed using bar plots and survival analysis based on various TIC subtype levels. The correlations between the TIC subtypes and the prognosis-related IRGs were visualized using the 'corrplot' package.

2.8. Analysis of drug sensitivity and immune checkpoints

The half maximal inhibitory concentration (IC50) was calculated by ridge regression using the 'oncoPredict' package to predict the drug treatment response and evaluate the therapeutic effects of chemotherapeutic drugs in patients with HNSCC. This package allowed the virtual prediction of drug response based on mRNA expression data in cell lines or patients with tumors [18]. The lower the IC50 value was, the better the drug sensitivity. The correlation between drug sensitivity and the RS was visualized using the 'ggExtra' package. We compared the
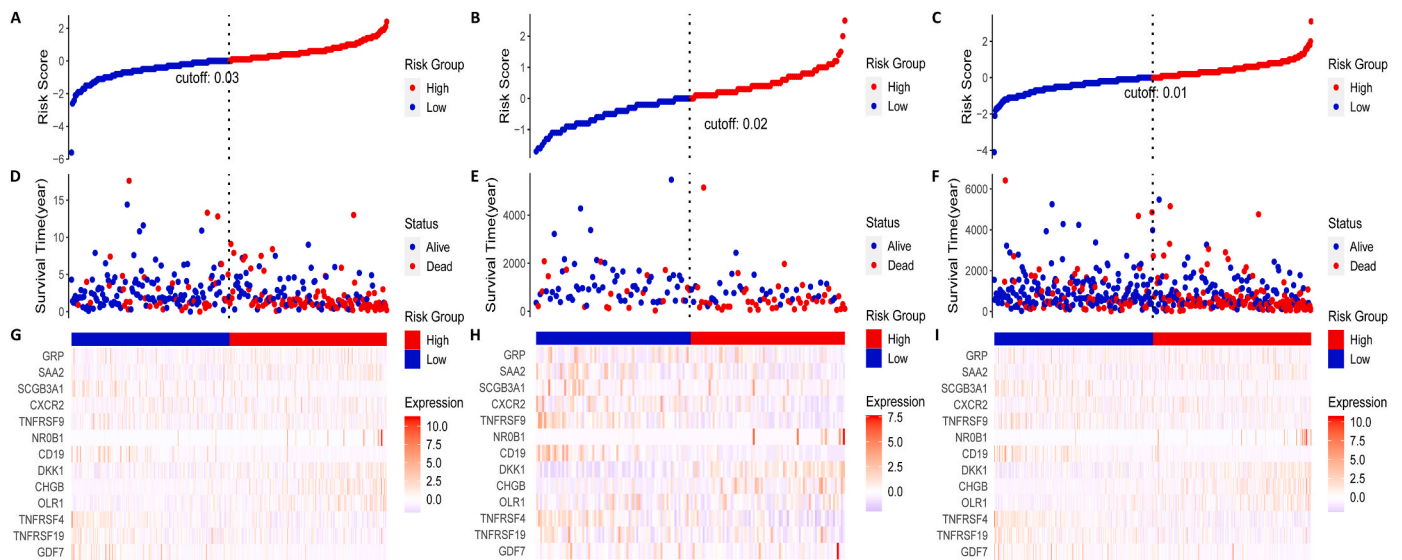
Fig. 4. Construction and cross-validation of prognostic model for HNSCC. (A-C) Distribution of RS for each sample in training, test and combined set, respectively. (D-F) Distribution of survival status for each sample in these three datasets. (G-I) The expression levels of the selected genes by heat map in the prognostic model for each sample in these three datasets.
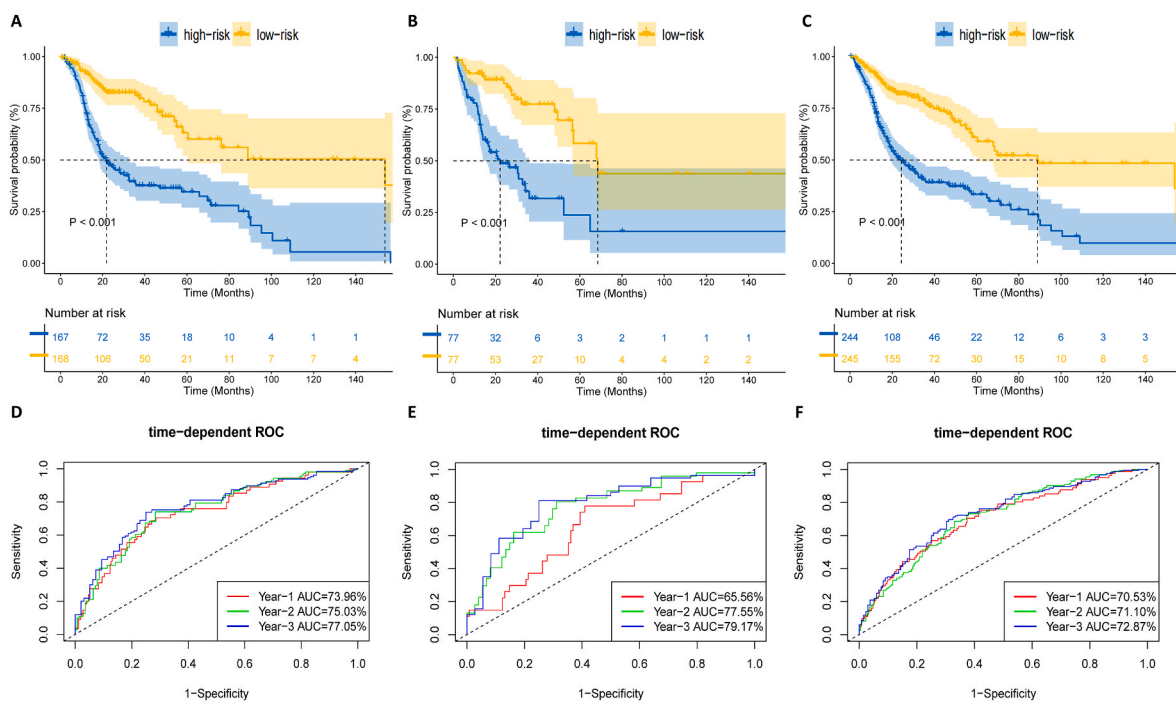

Fig. 5. Survival analysis of HNSCC and time-dependent ROC curves analysis for prognostic model. (A-C) K-M curves of HNSCC patients with high- and low-RS in the training, test and combined set, respectively. (D-F) time-dependent ROC curves analysis at 1-, 2- and 3-years in the training, test and combined set, respectively.

differential expression of immune checkpoints such as PD-1, PD-L1, PD-L2, CTLA4, and TIGIT in the high-risk and low-risk HNSCC groups. We also assessed the EGFR differential expression in various RS levels to improve our understanding of EGFR-targeted drug therapy in HNSCC.

2.9. Statistical analysis

R software (version 4.2.1) was used for statistical analysis and graph visualization. Statistical significance was set at $p < 0.05$. The prognostic prediction value was assessed using Cox regression analysis. K-M survival analysis was performed using the log-rank test. Two-group comparisons were conducted using the Wilcoxon rank sum test. Spearman's

test was used for correlation analysis. C-index and Akaike information criterion (AIC) were used for model selection.

3. Results

3.1. Immune-related DEG identification and functional enrichment analysis

There were 3946 DEGs, 1774 up-regulated and 2172 down-regulated (Fig. 1A). We detected 381 immune-related DEGs by intersecting the DEGs with 1793 IRGs in the ImmPort database (Fig. 1B). Subsequently, we used a heatmap to visualize the difference in the related IRG
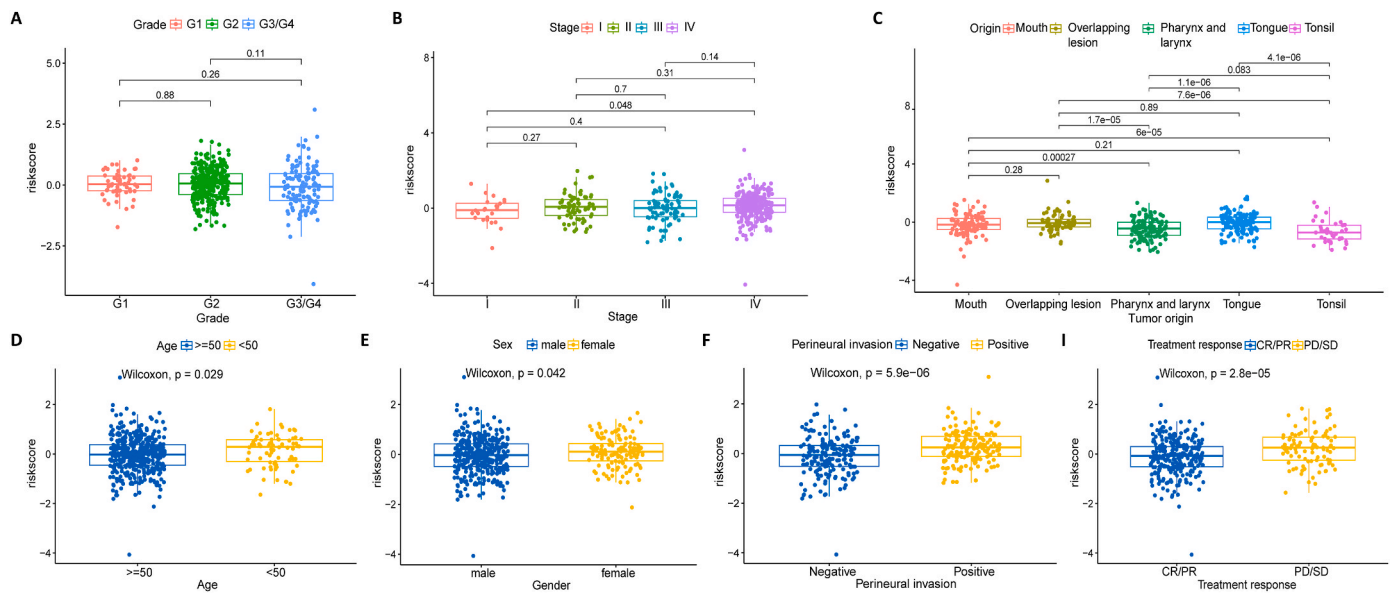
Fig. 6. Correlation analysis between clinical characteristics and the RS. (A-C) The correlation of RS among different tumor grades, stages and tumor origin of HNSCC. (D-I) The relationship between RS and age, sex, perineural invasion and treatment response.

expression between normal and tumor tissues in patients with HNSCC in association with their clinical characteristics (Fig. 1C). GO enrichment analysis showed that the mainly enriched immune-related DEGs in this study were associated with receptor-ligand activity, signaling receptor-activator activity, cytokine activity, cytokine-mediated signaling pathway, and cytokine receptor binding pathway (Fig. 2A). Cytokine-cytokine receptor interaction, neuroactive ligand-receptor interaction, JAK-STAT signaling pathway, PI3K-Akt signaling pathway, viral protein interaction with cytokine, and cytokine receptor pathway were mainly enriched based on the KEGG enrichment analysis (Fig. 2B).

3.2. Prognostic prediction model for HNSCC and cross-validation

Univariate Cox regression analysis screened prognostic IRGs in the Training Set (Table 1), the clinical characteristics of which are summarized in Table 2. The Training and Test sets were considered independent datasets due to the insignificant differences between them. We combined LASSO regression and the mSVM-RFE algorithm to construct various gene selection models (Fig. 3A-C). Genes selected by the various models within their concordance are summarized in Table S1. The model based on union analysis of LASSO regression and mSVM-RFE algorithm showed the highest C-index (Fig. 3D). The Coefficients of the 13 prognostic IRGs in this regression model are shown in Table 3.

The visualization of the RS distributions (Fig. 4A-C) and the relative survival statuses of the Training, Test, and combined sets showed higher mortality in the high-risk than low-risk patients (Fig. 4D-F). The IRG expression heatmaps indicated that six genes (*GRP, SAA2, NR0B1, DKK1, CHGB,* and *OLR1*) were slightly up-regulated in the high-risk group. The other genes were slightly down-regulated, suggesting that these IRGs might have the opposite effect on the prognostic model (Fig. 4G-I). A potential correlation was noted between the expression of cancer driver genes (*TP53, FAT1, NOTCH1, CSMD3,* and *CDKN2A*) and RS (Fig. S1).

The K-M analysis showed shorter OS in the high-risk group than the low-risk group in the Training, Test, and combined sets (Fig. 5A-C). Furthermore, time-dependent ROC curves showed that this predictive model had adequate prediction accuracy for the survival status. The areas under the curves for 1-, 2- and 3-year OS in the Training Set were 0.740, 0.750, and 0.771, respectively. Similar results were noted in the Test and combined sets (Fig. 5D-F).

3.3. Clinical characteristics in the various RS levels

We analyzed the correlation between the RS and various tumor grades, HNSCC stages, and tumor origins (Fig. 6A-C). Tumors arising from different locations showed different RS levels in most HNSCC kinds. However, the RS was not correlated with tumor grade or stage. Clinical characteristics, including age, sex, perineural invasion, and treatment response, were associated with the RS (Fig. 6D-I). Patients with a high RS were more likely to have perineural invasion and poor treatment response than those with low RS, indicating that the RS can reflect the tumor's biological behavior and outcomes.

The K-M curve in the subgroup analysis showed that females had much longer OS than males (Fig. 7A). The RS could divide the patients with HNSCC into high- and low-risk groups for the resection margin and perineural invasion (Fig. 7B and C). As for survival outcomes, the RS could distinguish between high- and low-risk patients for treatment response (Fig. 7D) and the need for radiation therapy (Fig. 7E). These results revealed that the present RS model had a considerable survival predicting value in association with sex, surgical status, treatment strategy, and treatment response.

3.4. Risk factors and nomogram construction

We performed univariate and multivariate Cox regression analyses for the correlation between clinical characteristics and the RS in association with OS to identify independent risk factors for poor HNSCC prognosis (Table 4). Univariate Cox regression analysis of the combined set found that age, stage, resection margin, perineural invasion, and the RS were risk factors associated with poor HNSCC prognosis. We also found that stage, positive resection margin, positive perineural invasion, and the RS were independent risk factors for poor HNSCC prognosis based on the multivariate Cox regression analysis. Results in the Training and Test sets also showed that the RS was an independent risk factor.

We constructed clinical nomograms to show the 1-, 2-, and 3-year OS in patients with HNSCC by combining the clinical features (including surgical status) and tumor risk factors (Fig. 8A). We selected the model with the highest C-index and the lowest AIC in the Training and Test sets (Table S2), which showed a high concordance and a good fitting. Calibration curves showed good agreement between the actual and nomogram-predicted 1-, 2-, and 3-year OS in the training and Test sets
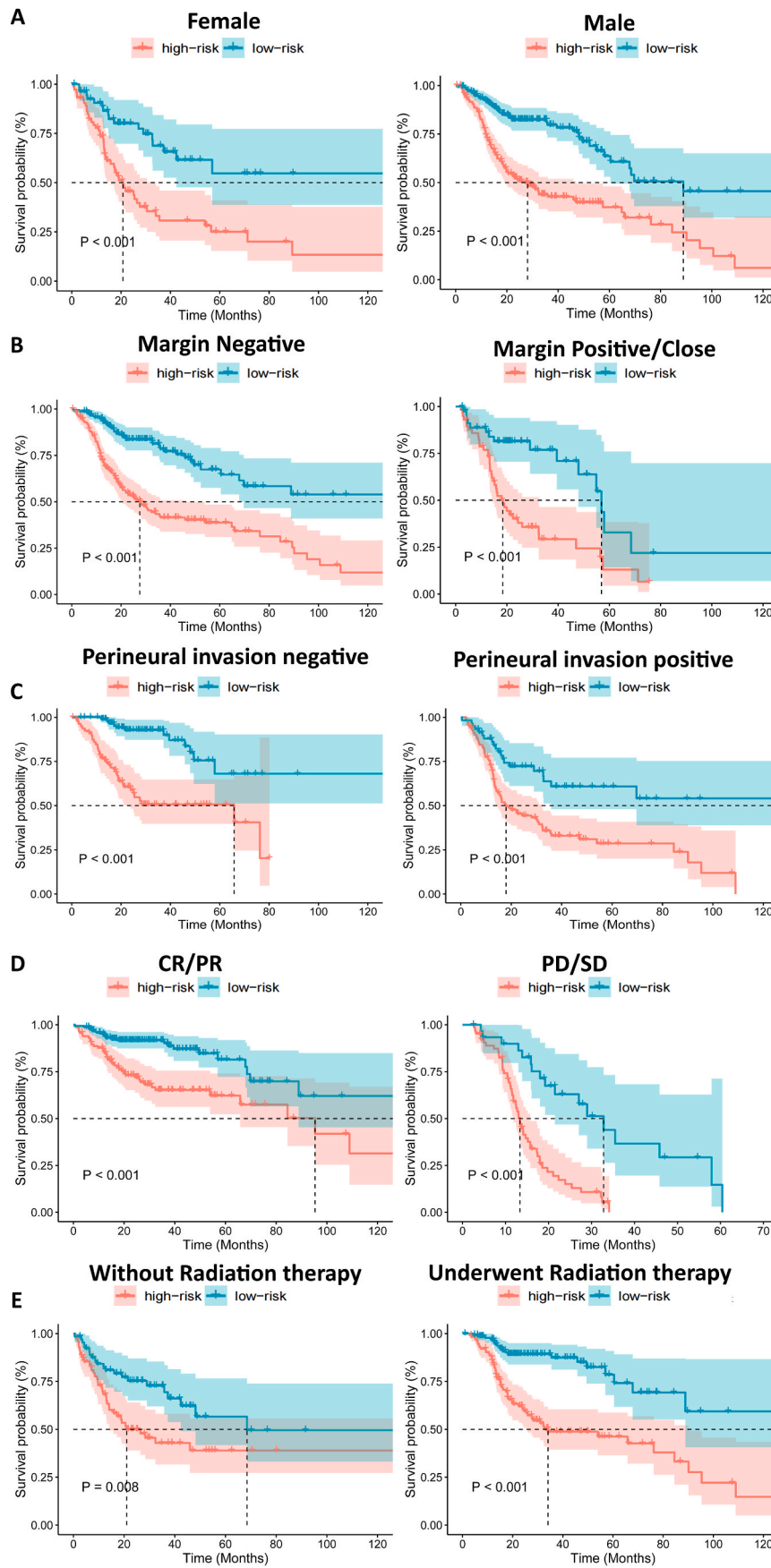
Fig. 7. K-M curve in subgroup analysis for patients with HNSCC. (A-E) K-M curve analysis for sex, resection margin, perineural invasion, treatment response and radiation therapy.

Table 4

Cox regression analysis of clinical characteristics and Riskscore for prognosis.

Data set	Item	Univariate-cox analysis		Multivariate-cox analysis	
		HR(95%CI)	p-value	HR(95%CI)	p-value
Training set	Age	1.026 (1.002-1.051)	0.036	1.018 (0.992-1.045)	0.172
	Male	0.799 (0.451-1.415)	0.441	1.685 (0.876-3.242)	0.118
	Grade	1.077 (0.707-1.641)	0.730	1.003 (0.626-1.606)	0.991
	Stage	1.406 (1.008-1.96)	0.045	1.376 (0.919-2.060)	0.121
	Margin positive	1.197 (0.661-2.167)	0.553	1.390 (0.723-2.674)	0.323
	Perineural invasion	2.279 (1.321-3.933)	0.003	2.134 (1.182-3.851)	0.012
	Radiation therapy	0.672 (0.400-1.127)	0.132	0.554 (0.298-1.030)	0.062
	Riskscore	4.215 (2.865-6.201)	0.000	4.392 (2.832-6.811)	0.000
Test set	Age	1.025 (0.985-1.067)	0.231	0.992 (0.943-1.044)	0.768
	Male	0.702 (0.308-1.604)	0.402	0.421 (0.157-1.129)	0.086
	Grade	2.577 (1.246-5.326)	0.011	2.784 (1.200-6.462)	0.017
	Stage	1.897 (0.996-3.613)	0.052	2.700 (1.047-6.961)	0.040
	Margin positive	4.210 (1.783-9.942)	0.001	1.763 (0.601-5.176)	0.302
	Perineural invasion	3.329 (1.438-7.707)	0.005	1.805 (0.708-4.600)	0.216
	Radiation therapy	0.586 (0.256-1.341)	0.206	0.281 (0.078-1.008)	0.052
	Riskscore	3.205 (1.732-5.930)	0.000	2.554 (1.296-5.034)	0.007
Combined set	Age	1.026 (1.005-1.047)	0.016	1.016 (0.994-1.040)	0.158
	Male	0.787 (0.495-1.252)	0.313	1.006 (0.607-1.666)	0.983
	Grade	1.312 (0.919-1.873)	0.135	1.271 (0.855-1.889)	0.235
	Stage	1.558 (1.160-2.093)	0.003	1.842 (1.289-2.632)	0.001
	Margin positive	1.742 (1.075-2.824)	0.024	1.696 (1.022-2.815)	0.041
	Perineural invasion	2.584 (1.627-4.105)	0.000	1.969 (1.221-3.174)	0.005
	Radiation therapy	0.692 (0.445-1.076)	0.102	0.413 (0.243-0.701)	0.001
	Riskscore	4.045 (2.860-5.723)	0.000	3.549 (2.453-5.132)	0.000

HR = hazard ratio; CI=Confidence interval.

(Fig. 8B-G).

3.5. TIC analysis, immune checkpoints, and drug sensitivity

The CIBERSORT algorithm analyzed the 22 TIC subtypes in HNSCC. The TIC subtypes in the high- and low-risk groups according to the predictive model were compared and visualized by a bar plot (Fig. 9A). The correlations of the 22 TIC subtypes in HNSCC and the prognostic IRGs were analyzed and visualized by correlation heatmap (Fig. 9B). Each TIC subtype was divided into high- and low-level groups based on the median level. We found survival differences in several TIC subtypes between these two groups (Fig. 9C-H). Patients with HNSCC with high levels of plasma cells, follicular helper T cells, and gamma delta T cells showed longer OS than their low-level counterparts, while those with high-level CD4 memory resting T cells had shorter OS. These results agreed with the abundance analysis of these four TIC subtypes in the various RS levels. High expression of *GDF7* and *CD19* and low expression of *DKK1* were observed in patients with high levels of plasma cells, follicular helper T cells, and gamma delta T cells. The opposite correlation was observed in CD4 memory resting T cells. As for the immune checkpoint analysis, the high-risk HNSCC subgroup showed higher expression levels of PD-L1 and PD-L2, while the low-risk HNSCC subgroup showed higher expression levels of PD-1, CTLA4, and TIGIT (Fig. 10A-E). We also showed that the high-RS group had a higher expression level of EGFR than the low-RS group (Fig. 10F), highlighting the benefits the high-risk HNSCC subgroup can gain from EGFR-targeted therapy. Drug sensitivity analysis for the high- and low-risk HNSCC subgroups and the lower IC50 values for the high-risk HNSCC subgroup were explored for Selumetinib, ERK_6604, ERK_2440, SCH772984, Trametinib, SB505124, Dasatinib, and PD0325901 (Fig. 11A-H). The results indicated that the high-risk HNSCC subgroup could benefit from these drugs. Correlation analysis between RS and IC50 values (Fig. 12A-H) indicated that the RS-based prognostic model of IRGs was related to drug sensitivity.

4. Discussion

Considering the high heterogeneity of HNSCC, it is necessary to establish a robust prediction model for risk stratification, TICs, prognosis, and guidance of personalized clinical treatment. The IRGs' expression in tumors was considered a convincing factor reflecting the immune status in tumor tissues and the TME [19]. Several predictive models based on immune-related signatures were highly accurate in HNSCC [12,13]. However, differences in IRGs' screening and variable immune-related signature selection made the prediction value of such predictive models and stratification using risk factors derived from them controversial and with limited clinical decision-making value.

We screened the HNSCC samples and identified IRGs using LASSO regression and the mSVM-RFE algorithm to establish a novel model to predict HNSCC prognosis with high concordance and moderate model complexity. The prediction performance of this predictive model was slightly higher than that of previously published models [12,13]. Higher expression of *FAT1 and CSMD3 and lower expression of NOTCH1, CDKN2A,* and *TP53* were associated with higher RS in HNSCC, suggesting that the expression of IRGs might be influenced by cancer driver genes. Furthermore, high stratification risk factor values in our model were noted in age, sex, tumor location, resection margin, perineural invasion, treatment response, and radiation therapy. Positive resection margin in initial treatment for HNSCC indicated worse outcome and tumor control and increased risk of perineural invasion [15–20]. Our results indicated that patients with high-risk HNSCC and a positive resection margin showed worse survival than those with low-risk HNSCC or a negative resection margin. Similar results were observed
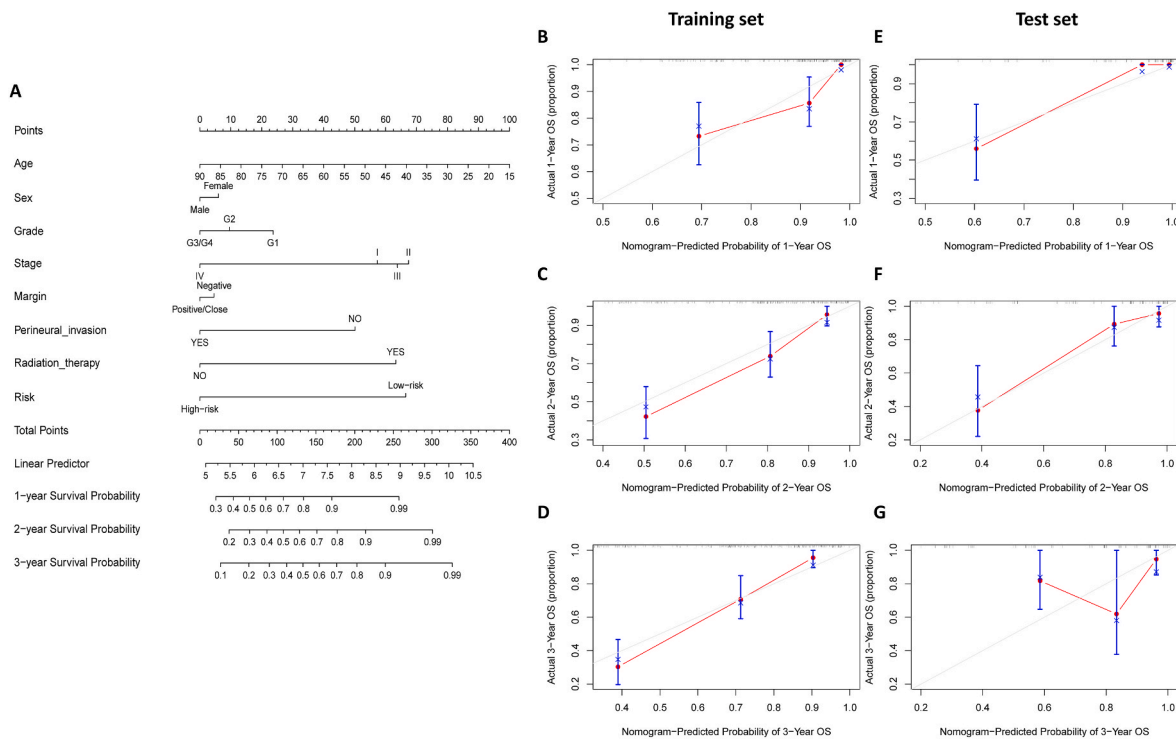
Fig. 8. Establishment and validation of nomogram model. (A) The nomogram model combined with clinical characteristics, surgical status and tumor risk. (B-G) Calibration curves of the nomogram for 1-, 2- and 3- years in training and test set, respectively.
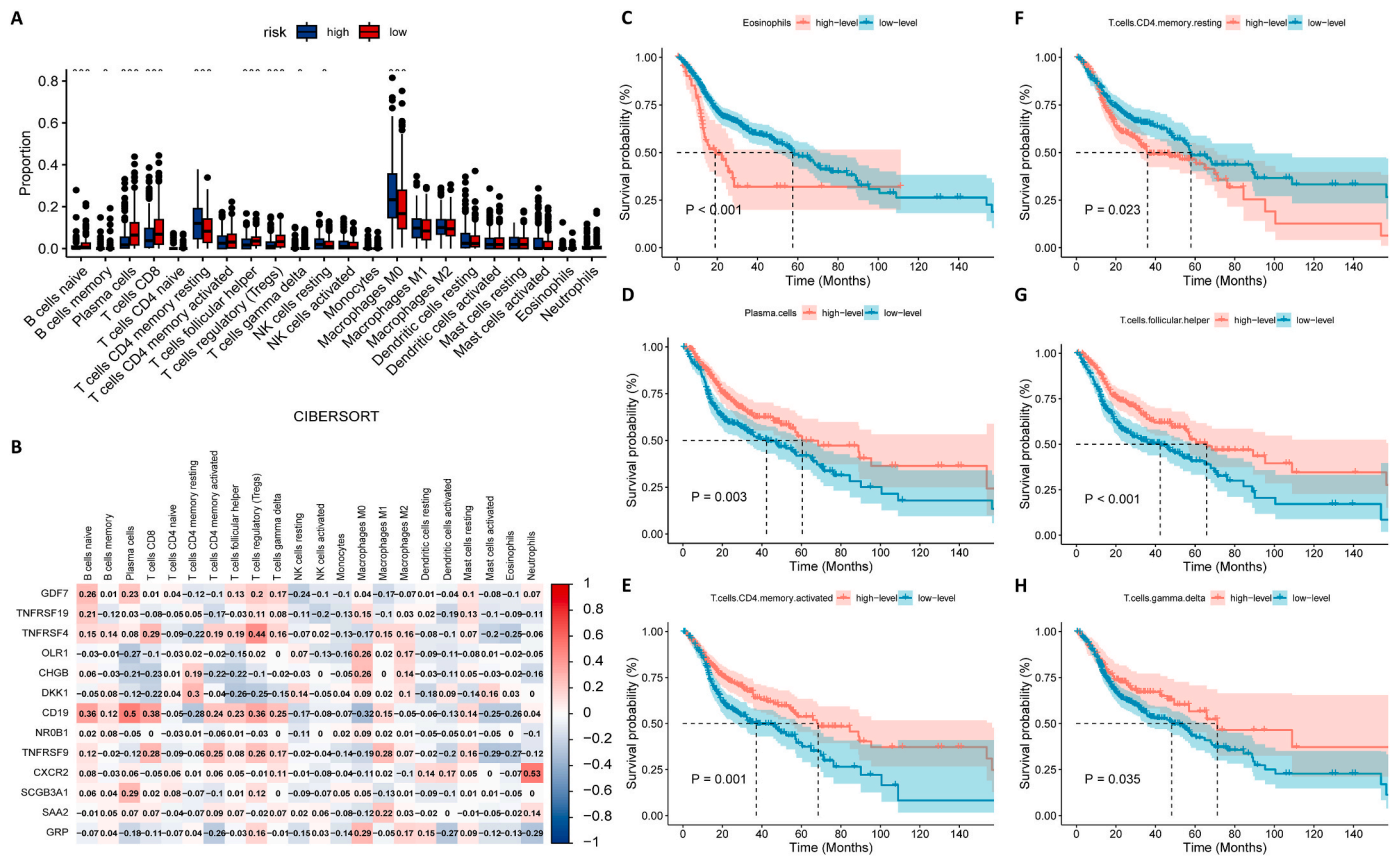

Fig. 9. TICs analysis of HNSCC. (A) Bar plot showing the difference of 22 TIC subtypes in HNSCC for the high-/low-risk groups. (B) The correlation heat map of the 22 TIC subtypes in HNSCC and the selected IRGs. (C-H) Six TICs showed effect on survival outcome for patients with HNSCC.
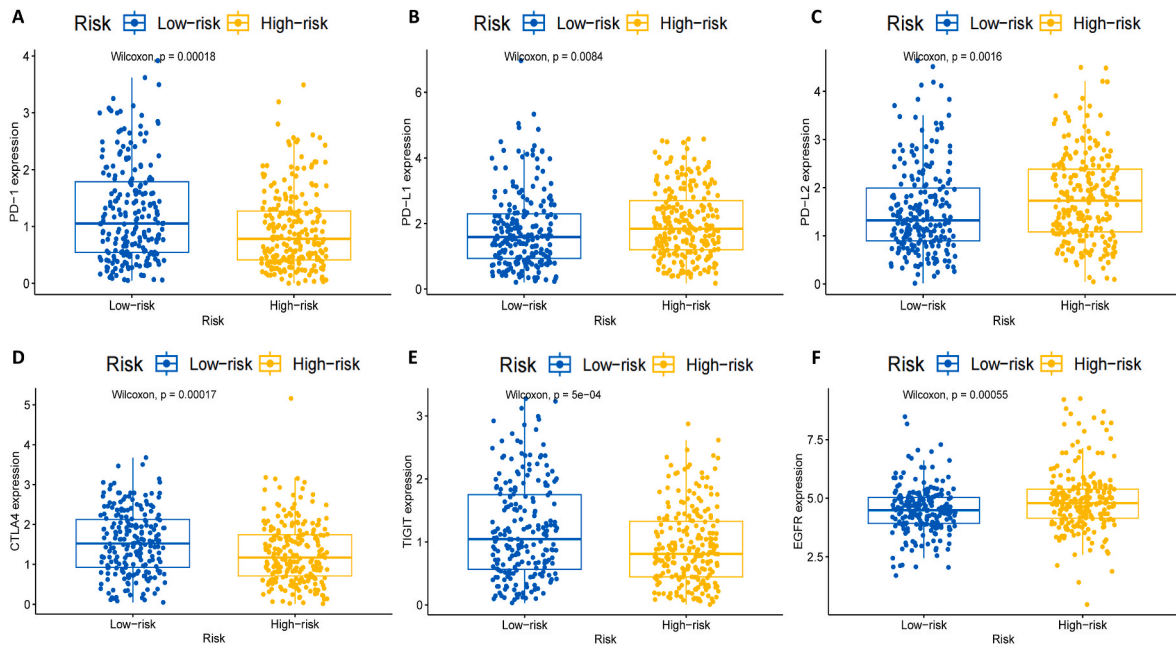
Fig. 10. Comparison of the expression levels of therapeutic targets of high- and low-risk groups. (A-F) PD-1, PD-L1, PD-L2, CTLA4, TIGIT and EGFR,respectively.
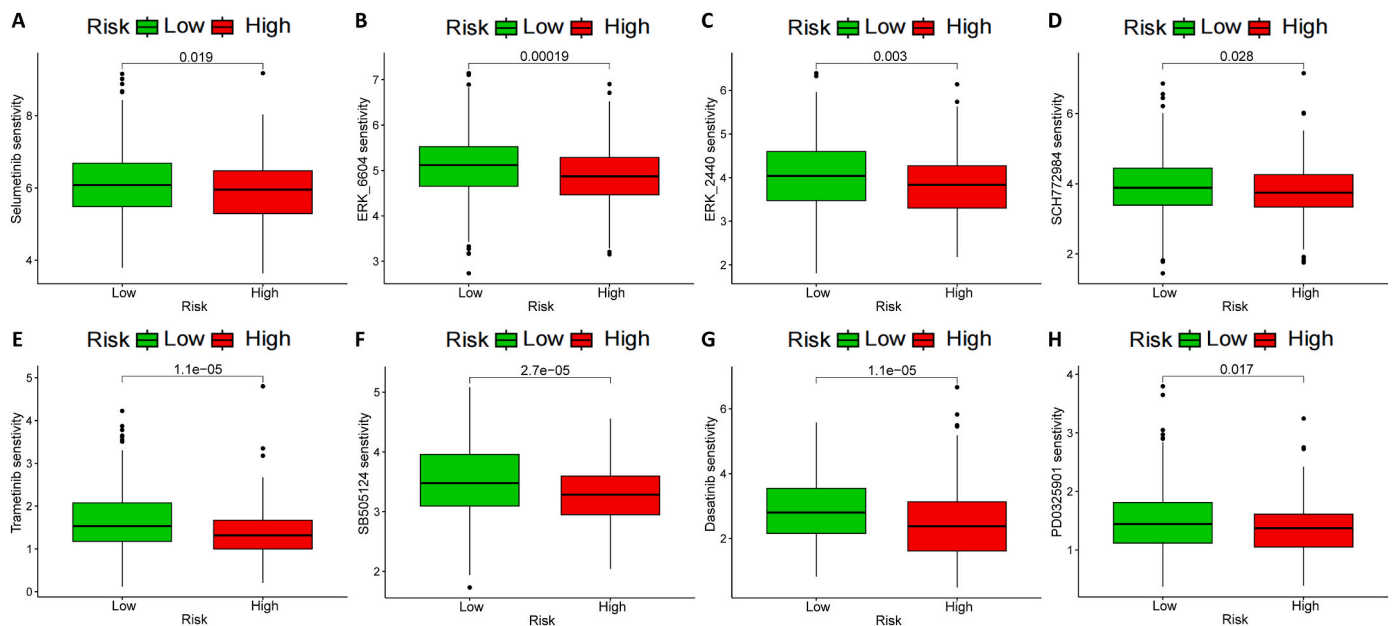

Fig. 11. Comparison of the levels of IC50 of high- and low-risk groups in different drugs. (A-H) Selumetinib, ERK_6604, ERK_2440, SCH772984, Trametinib, SB505124, Dasatinib and PD0325901, respectively.

for perineural invasion in both the high- and low-risk groups. Radiation therapy is a widely used treatment for HNSCC. It is necessary to screen prognostic biomarkers to develop personalized radiotherapy approaches [21]. Our results suggested that both high- and low-risk HNSCC subgroups could benefit from radiotherapy, especially low-risk patients. High RS values were associated with a non-responding disease during follow-up. Together, these results indicated that the developed predictive model could be valuable for personalized treatment strategies for patients with HNSCC.

HNSCC is assumed to cause severe immunosuppression, resulting in poor prognosis [6]. The immunosuppressive effect, associated with the surgical approach and radiotherapy, was correlated with the tumor's immune response quality and could affect survival and treatment

outcomes [22]. Therefore, we constructed a predictive nomogram model that included radiotherapy and surgical status. We believe such a model could reflect real-world clinical conditions. The nomogram model, chosen based on its C-index and AIC, showed higher accuracy and better fitting than nomograms containing only basic clinical characteristics and RS. Improving the primary treatment outcomes by decreasing the immune-suppressive TME is important. The TIC abundance and survival analyses revealed that four prognosis-related cell subtypes, plasma cell, CD4 memory resting T cells, follicular helper T cells, and gamma delta T cells, were associated with the RS level. Most of these cells were T lymphocytes, assumed to promote tumor progression and restrain tumor regression by chronic inflammation. These effects might be associated with out-of-balance neuro-hormones.
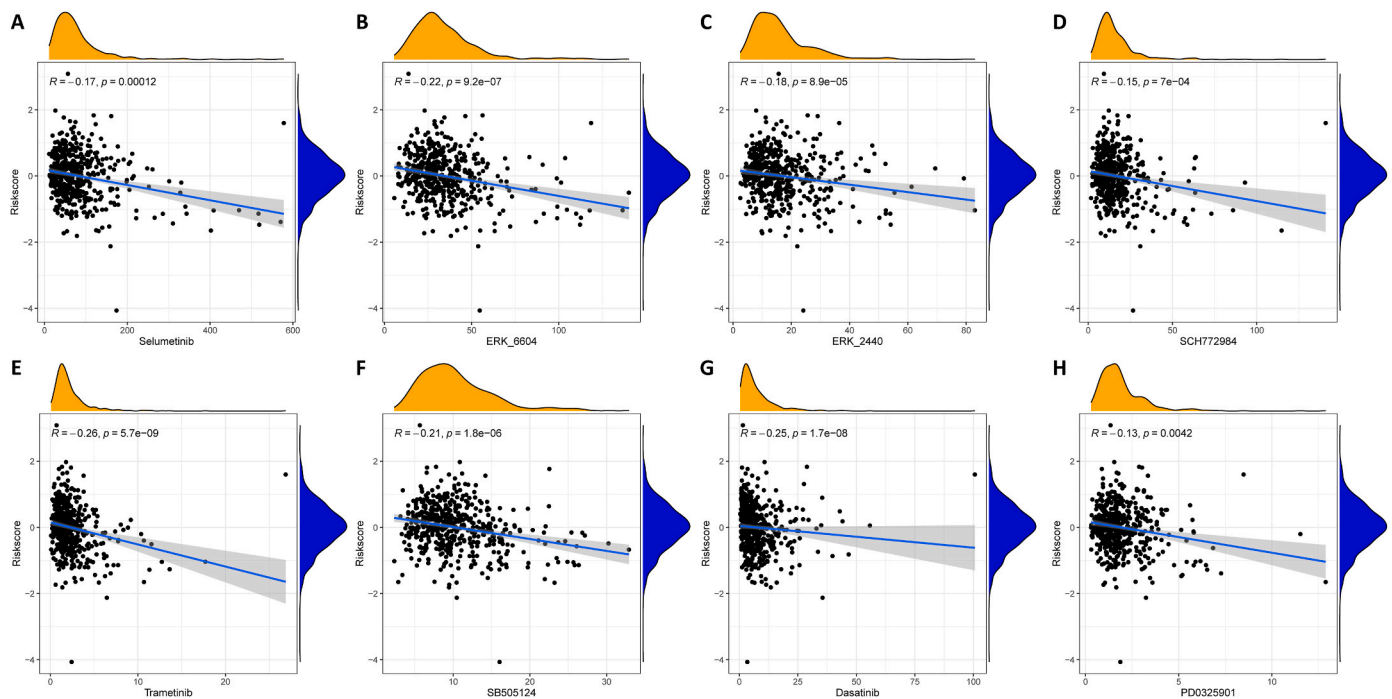
Fig. 12. Correlation between RS and IC50 values in different drugs. (A-H) Selumetinib, ERK_6604, ERK_2440, SCH772984, Trametinib, SB505124, Dasatinib and PD0325901, respectively.

Neuroendocrine factors, such as nitric oxide, are produced by both tumor cells and TICs in all HNSCC tumor subtypes. This might promote adhesion and vascular endothelial cell permeability, allowing metastasis and promoting T-helper lymphocyte expansion [9,23]. Plasma cell infiltration was considered a positive predictor of the prognosis and immunotherapy response in many tumors. Their infiltration also promotes the excretion of immunosuppressive cytokines to reduce the infiltration of effector T cells [24]. The CD4 memory resting T cells affected T cell receptor signaling and CD4$^+$ T cell activation by N-glycans and were associated with cell adhesion, tumor immunity, and metastasis [25]. Follicular helper T cell infiltration was shown to promote immune activation of TME and promote tumor killing, indicating a good prognosis in HNSCC [26]. Similarly, as immune-activated cells, gamma delta T cell enrichment was observed in TME, with a high expression of immune-positive regulatory chemokines in non-small cell lung cancer [27]. In our study, *GDF7*, *DKK1*, and *CD19* expression rates were associated with these TICs and the RS distribution. *DKK1* regulates the TME and immune response in HNSCC and is a negative survival predictor [13]. *CD19* is a co-receptor of antigen receptors and is associated with signal transduction for B-cells and proliferation regulation of tumor cells. *CD19* downregulation was related to a worse prognosis for patients with HNSCC [28]. *GDF7*, highly expressed in bladder cancer, was considered a ligand of the TGF-β superfamily and the T-cell exhaustion gene and a predictor of poor prognosis [29]. Therefore, our results showed that these three IRGs could affect the TME regulation of HNSCC.

Immunotherapy and EGFR-targeted drugs are widely used to treat locally advanced HNSCC. However, considering the ICI objective response rate limitation and the controversy concerning the role of immunotherapy in multimodal treatments, further analysis for certain HNSCC subsets is needed [5,6]. Higher expression levels of PD-1, CTLA4, and TIGIT in the low-risk group indicated that patients with low-risk HNSCC could benefit from several ICIs, including nivolumab, pembrolizumab, and ipilimumab. TIGIT blockade, a novel therapy for HNSCC, might enhance the response rate for anti-PD-1/PD-L1 therapy [30]. Our results provided new insights into dual-targeting treatment for patients with low-risk HNSCC. The higher expression of PD-L1, PD-L2,

and EGFR in the high-risk group indicated that patients with high-risk HNSCC might benefit from anti-PD-L1 (e.g., durvalumab or atezolizumab) and anti-EGFR (e.g., cetuximab) drugs. Although clinical trials about anti-PD-L2 immunotherapy are unavailable, PD-L2 expression was crucial to predict therapeutic outcomes [31]. Cisplatin-based chemotherapy is widely used for HNSCC; however, the rapid development of drug resistance remains a serious challenge [6]. According to our RS model, patients with high-risk HNSCC are highly sensitive to many MAPK signaling pathway inhibitors, including PD0325901, Selumetinib, ERK_6604, ERK_2440, SCH772984, and Trametinib. These results were similar to those of Zhang et al. [32], who investigated the resistance to these MAPK signaling pathway inhibitors in patients with prostate cancer. The efficacy and regulation of MAPK signaling pathway inhibitors in HNSCC require further investigation of their association with IRGs' expression. Although high-risk HNSCC showed high sensitivity to dasatinib, an Src family kinase inhibitor, combination treatment might show even higher therapeutic potential [33]. As a TGF-β inhibitor, SB-505124 showed a potential therapeutic effect in pediatric acute myeloid leukemia and bone metastases [34,35]. Our results provided new insights into drug selection for high-risk HNSCC. However, since the drug sensitivity analysis results were calculated based on cell lines' expression data, their interpretation should be made cautiously.

Our study had several limitations. First, we used retrospective data from TCGA database; therefore, external validation data are needed to confirm our findings. Second, the mechanisms through which the 13 IRGs contribute to tumorigenesis and HNSCC progression need further exploration and verification by fundamental experiments. Third, large-sample multi-center prospective studies are needed to assess the clinical value of our model. Finally, further clinical trials are needed to validate the treatment responses based on our drug sensitivity analysis.

In conclusion, we developed and validated a novel predictive model for patients with HNSCC based on IRGs. A nomogram with surgical status was constructed to predict survival. The RS could be a stable indicator for HNSCC therapy, helping evaluate TICs and immunotherapy targets and possibly predict drug sensitivity and efficacy.

Authors' contributions

Chenglong Wang conceived and designed the work. Lang Wang and Xianchao Yu carried out the software coding and data analysis. Lang Wang and Hongwei Li prepared all the tables and figures. Lang Wang, Xianchao Yu and Hongwei Li wrote the manuscript. Chenglong Wang critically reviewed the codes and the manuscript. All authors read and approved the final manuscript.

Funding

Declaration of competing interest

The authors declare that they have no known competing financial interests or personal relationships that could have appeared to influence the work reported in this paper.

Data availability

Data will be made available on request.

Acknowledgement

Appendix A. Supplementary data

Supplementary data to this article can be found online at https://doi.org/10.1016/j.bbrep.2023.101557.

References

[1] L.Q.M. Chow, Head and neck cancer, N. Engl. J. Med. 382 (1) (2020) 60–72, https://doi.org/10.1056/NEJMra1715715.

[2] A. Karimi, E. Mohebbi, S. Mckay-Chopin, H. Rashidian, M. Hadji, V. Peyghambari, et al., Human papillomavirus and risk of head and neck squamous cell carcinoma in Iran, Microbiol. Spectr. 10 (4) (2022), e0011722, https://doi.org/10.1128/spectrum.00117-22.

[3] C. Carazo-Casas, R. Gil-Prieto, V. Hernández-Barrera, Á. Gil de Miguel, Trends in hospitalization and death rates among patients with head and neck cancer in Spain, 2009 to 2019, Hum. Vaccines Immunother. 18 (5) (2022), 2082192, https://doi.org/10.1080/21645515.2022.2082192.

[4] H. Sung, J. Ferlay, R.L. Siegel, M. Laversanne, I. Soerjomataram, A. Jemal, et al., Global cancer statistics 2020: GLOBOCAN estimates of incidence and mortality worldwide for 36 cancers in 185 countries, CA A Cancer J. Clin. 71 (3) (2021) 209–249, https://doi.org/10.3322/caac.21660.

[5] Y.J. Rao, J.F. Goodman, F. Haroun, J.E. Bauman, Integrating immunotherapy into multimodal treatment of head and neck cancer, Cancers 15 (3) (2023) 672, https://doi.org/10.3390/cancers15030672.

[6] X. Wang, J. Guo, P. Yu, L. Guo, X. Mao, J. Wang, et al., The roles of extracellular vesicles in the development, microenvironment, anticancer drug resistance, and therapy of head and neck squamous cell carcinoma, J. Exp. Clin. Cancer Res. 40 (1) (2021) 35, https://doi.org/10.1186/s13046-021-01840-x.

[7] L.R.C. Castellano, S.B.S.C. Cruz, M. Hier, P.R.F. Bonan, M.A. Alaoui-Jamali, S.D. da Silva, Implications and emerging therapeutic avenues of inflammatory response in HPV+ head and neck squamous cell carcinoma, Cancers 14 (21) (2022) 5406, https://doi.org/10.3390/cancers14215406.

[8] M.P.S. Damasio, C.S. Nascimento, L.M. Andrade, V.L. de Oliveira, C.E. Calzavara-Silva, The role of T-cells in head and neck squamous cell carcinoma: from immunity to immunotherapy, Front. Oncol. 12 (2022), 1021609, https://doi.org/10.3389/fonc.2022.1021609.

[9] R.M. Slominski, C. Raman, J.Y. Chen, A.T. Slominski, How cancer hijacks the body's homeostasis through the neuroendocrine system, Trends Neurosci. 46 (4) (2023) 263–275, https://doi.org/10.1016/j.tins.2023.01.003.

[10] H. Wu, X. Zhao, T. Zhu, D. Rong, Y. Wang, D. Leng, et al., A glycosyltransferase-related signature for predicting overall survival in head and neck squamous cell carcinoma, Front. Genet. 13 (2022), 856671, https://doi.org/10.3389/fgene.2022.856671.

[11] T. Ettl, M. Grube, D. Schulz, R.J. Bauer, Checkpoint inhibitors in cancer therapy: clinical benefits for head and neck cancers, Cancers 14 (20) (2022) 4985, https://doi.org/10.3390/cancers14204985.

[12] F. Zhang, Y. Liu, Y. Yang, K. Yang, Development and validation of a fourteen-innate immunity-related gene pairs signature for predicting prognosis head and neck squamous cell carcinoma, BMC Cancer 20 (1) (2020) 1015, https://doi.org/10.1186/s12885-020-07489-7.

[13] Y. Zhang, P. Chen, Q. Zhou, H. Wang, Q. Hua, J. Wang, et al., A novel immune-related prognostic signature in head and neck squamous cell carcinoma, Front. Genet. 12 (2021), 570336, https://doi.org/10.3389/fgene.2021.570336.

[14] Y. Fan, J. Wang, Y. Wang, Y. Li, S. Wang, Y. Weng, et al., Development and clinical validation of a novel 5 gene signature based on fatty acid metabolism-related genes in oral squamous cell carcinoma, Oxid. Med. Cell. Longev. 2022 (2022), 3285393, https://doi.org/10.1155/2022/3285393.

[15] J. Zhu, R. Zhou, Y. Wang, M. Yu, Perineural invasion as a prognostic factor in head and neck squamous cell carcinoma: a systematic review and meta-analysis, Acta Otolaryngol. 139 (11) (2019) 1038–1043, https://doi.org/10.1080/00016489.2019.1655167.

[16] S. Wang, J.H. Ying, H. Xu, Identification of diagnostic biomarkers associated with stromal and immune cell infiltration in fatty infiltration after rotator cuff tear by integrating bioinformatic analysis and machine-learning, Int. J. Gen. Med. 15 (2022) 1805–1819, https://doi.org/10.2147/IJGM.S354741.

[17] A.M. Newman, C.L. Liu, M.R. Green, A.J. Gentles, W. Feng, Y. Xu, et al., Robust enumeration of cell subsets from tissue expression profiles, Nat. Methods 12 (5) (2015) 453–457, https://doi.org/10.1038/nmeth.

[18] D. Maeser, R.F. Gruener, R.S. Huang, oncoPredict: an R package for predicting in vivo or cancer patient drug response and biomarkers from cell line screening data, Briefings Bioinf. 22 (6) (2021) bbab260, https://doi.org/10.1093/bib/bbab260.

[19] C. Ji, Y. Wang, Y. Wang, J. Luan, L. Yao, Y. Wang, et al., Immune-related genes play an important role in the prognosis of patients with testicular germ cell tumor, Ann. Transl. Med. 8 (14) (2020) 866, https://doi.org/10.21037/atm-20-654.

[20] B. Coutu, E. Ryan, D. Christensen, E. Lawrence, E.B. Bell, W. Zhen, et al., Positive margins matter regardless of subsequent resection findings, Oral Oncol. 128 (2022), 105850, https://doi.org/10.1016/j.oraloncology.2022.105850.

[21] A. Rühle, J. Todorovic, S.S.K. Spohn, E. Gkika, C. Becker, A. Knopf, et al., Prognostic value of tumor-infiltrating immune cells and immune checkpoints in elderly head-and-neck squamous cell carcinoma patients undergoing definitive (chemo)radiotherapy, Radiat. Oncol. 17 (1) (2022) 181, https://doi.org/10.1186/s13014-022-02153-9.

[22] O. Bakos, C. Lawson, S. Rouleau, L.H. Tai, Combining surgery and immunotherapy: turning an immunosuppressive effect into a therapeutic opportunity, J Immunother Cancer 6 (1) (2018) 86, https://doi.org/10.1186/s40425-018-0398-7.

[23] I. Solomon, V.M. Voiculescu, C. Caruntu, M. Lupu, A. Popa, M.A. Ilie, et al., Neuroendocrine factors and head and neck squamous cell carcinoma: an affair to remember, Dis. Markers 2018 (2018), 9787831, https://doi.org/10.1155/2018/9787831.

[24] X. Xie, C.X. Dou, M.R. Luo, K. Zhang, Y. Liu, J.W. Zhou, et al., Plasma cell subtypes analyzed using artificial intelligence algorithm for predicting biochemical recurrence, immune escape potential, and immunotherapy response of prostate cancer, Front. Immunol. 13 (2022), 946209, https://doi.org/10.3389/fimmu.2022.946209.

[25] C. Zheng, L. Sun, B. Zhou, A. Wang, Identification and validation of a metabolism-related model and associated with tumor-infiltrating lymphocytes in p53 mutant lung adenocarcinoma patients, Ann. Transl. Med. 9 (16) (2021) 1312, https://doi.org/10.21037/atm-21-3234.

[26] L. Dong, Q. Sun, F. Song, X. Song, C. Lu, Y. Li, et al., Identification and verification of eight cancer-associated fibroblasts related genes as a prognostic signature for head and neck squamous cell carcinoma, Heliyon 9 (3) (2023), e14003, https://doi.org/10.1016/j.heliyon.2023.e14003.

[27] Y. Sun, Q. Yang, J. Shen, T. Wei, W. Shen, N. Zhang, et al., The effect of smoking on the immune microenvironment and immunogenicity and its relationship with the prognosis of immune checkpoint inhibitors in non-small cell lung cancer, Front. Cell Dev. Biol. 9 (2021), 745859, https://doi.org/10.3389/fcell.2021.745859.

[28] S. Li, Y. Wang, R. Sun, D. Franceschi, H. Pan, C. Wei, et al., Single-cell transcriptome analysis reveals different immune signatures in HPV- and HPV + driven human head and neck squamous cell carcinoma, J Immunol Res 2022 (2022), 2079389, https://doi.org/10.1155/2022/2079389.

[29] W. Xu, H.J. Tang, A. Anwaier, W. Liu, X. Tian, J. Su, et al., Immunogenomic characteristics of cell-death-associated genes with prognostic implications in bladder cancer, Front. Immunol. 13 (2022), 909324, https://doi.org/10.3389/fimmu.2022.909324.

[30] L. Mao, Y. Xiao, Q.C. Yang, S.C. Yang, L.L. Yang, Z.J. Sun, TIGIT/CD155 blockade enhances anti-PD-L1 therapy in head and neck squamous cell carcinoma by targeting myeloid-derived suppressor cells, Oral Oncol. 121 (2021), 105472, https://doi.org/10.1016/j.oraloncology.2021.105472.

[31] Y. Wang, J. Du, Z. Gao, H. Sun, M. Mei, Y. Wang, et al., Evolving landscape of PD-L2: bring new light to checkpoint immunotherapy, Br. J. Cancer 128 (7) (2023) 1196–1207, https://doi.org/10.1038/s41416-022-02084-y.

[32] P. Zhang, H. Gao, C. Ye, R. Yan, L. Yu, C. Xia, et al., Large-scale transcriptome data analysis identifies KIF2C as a potential therapeutic target associated with immune infiltration in prostate cancer, Front. Immunol. 13 (2022), 905259, https://doi.org/10.3389/fimmu.2022.905259.

[33] C.E. Lehman, A. Spencer, S. Hall, J.J.P. Shaw, J. Wulfkuhle, E.F. Petricoin, et al., IGF1R and Src inhibition induce synergistic cytotoxicity in HNSCC through

inhibition of FAK, Sci. Rep. 11 (1) (2021), 10826, https://doi.org/10.1038/s41598-021-90289-1.

[34] Y. Tao, L. Wei, H. You, Ferroptosis-related gene signature predicts the clinical outcome in pediatric acute myeloid leukemia patients and refines the 2017 ELN classification system, Front. Mol. Biosci. 9 (2022), 954524, https://doi.org/10.3389/fmolb.2022.954524.

[35] B. Wang, J. Bai, B. Tian, H. Chen, Q. Yang, Y. Chen, et al., Genetically engineered hematopoietic stem cells deliver TGF-β inhibitor to enhance bone metastases immunotherapy, Adv. Sci. 9 (28) (2022), e2201451, https://doi.org/10.1002/advs.202201451.